Popular summary for

Three way comparison between two OMI/Aura and one POLDER/PARASOL cloud pressure products

Sneep, M., J. F. de Haan, P. Stammes, C. Vanbauce, J. Joiner, A. P. Vasilkov, and P. F. Levelt,

Satellite-based measurements of the Earth's atmosphere and surface are very important because they help us understand our planet's climate, monitor global air quality, and predict the weather. Almost all of these measurements are affected by clouds. Some instruments are designed specifically to study how clouds impact climate. For other measurements, clouds can either be a nuisance or they may actually help us to extract information about gases in the atmosphere. In all cases, it is important to understand exactly how clouds impact the satellite observations.

Ozone is an important constituent of the Earth's atmosphere, and it is a focus of several space-based instruments. It acts as a protective shield by absorbing ultraviolet rays high in the atmosphere. But ozone in the atmosphere near the Earth's surface can also be harmful to life. It damages lung tissue when inhaled and can create visible scars on plants. It is important to be able to determine how much ozone is in the upper atmosphere where it is crucial to our survival and how much is in the lower atmosphere where it is considered to be a pollutant.

Satellites are extremely useful for measuring ozone globally. However, satellite instruments do not directly sample the Earth's atmosphere. Instead, they make measurements in different wavelengths of light either reflected from the sun by the atmosphere, clouds, and surface or emitted as heat. The measured wavelengths include colors that we can see, invisible light that can burn our skin, and heat (including microwaves) from the atmosphere, surface, and clouds. Because clouds are good reflectors of light, they can shield the lower part of the atmosphere from satellite instruments. We can use this property and the fact that clouds vary in height to slice up the atmosphere and tell us where exactly the ozone is. But first we must understand precisely how clouds affect the incoming sunlight.

There are currently 5 satellites flying in a formation; They observe the same regions of the Earth's atmosphere within minutes of each other. This formation is known as the A-train because the first satellite is named Aqua and the caboose is called Aura. Both Aqua and Aura are part of NASA's Earth Observing System. One of the middle cars, called Parasol, carries an instrument that can determine the height of a cloud using the absorption of sunlight by atmospheric oxygen. Aura has an instrument that can make similar measurements using two completely independent techniques. This paper shows that all three techniques provide similar estimates of the cloud height. Some of the small differences can be traced to features of the individual retrieval algorithms. This comparison serves as a means of validating our algorithms.

Three way comparison between OMI/Aura and POLDER/PARASOL cloud pressure products

M. Sneep[1], J. F. de Haan[1], P. Stammes[1], C. Vanbauce[2], J. Joiner[3],

A. P. Vasilkov[4], and P. F. Levelt[1]

[1]Climate Research and Seismology Department, Royal Netherlands Meteorological Institute (KNMI), De Bilt, Netherlands.

[2]Laboratoire d'Optique Atmosphérique, Université des Sciences et Technologies de Lille, CNRS, Lille, France.

[3]National Aeronautics and Space Administration, Goddard Space Flight Center, Greenbelt, MD 20771 USA.

[4]Science Systems and Applications, Inc., Lanham, MD 20706 USA.

0148-0227/07/$9.00

Abstract. The cloud pressures determined by three different algorithms, operating on reflectances measured by two space-borne instruments in the "A" train, are compared with each other. The retrieval algorithms are based on absorption in the oxygen A-band near 760 nm, absorption by a collision induced absorption in oxygen near 477 nm, and the filling in of Fraunhofer lines by rotational Raman scattering. The first algorithm operates on data collected by the POLDER instrument on board PARASOL, while the latter two operate on data from the OMI instrument on board Aura. The satellites sample the same air mass within about 15 minutes.

Using one month of data, the cloud pressures from the three algorithms are found to show a similar behavior, with correlation coefficients larger than 0.85 between the data sets for thick clouds. The average differences in the cloud pressure are also small, between 2 and 45 hPa, for the whole data set. For optically thin to medium thick clouds, the cloud pressure the distribution found by POLDER is very similar to that found by OMI using the O_2–O_2 absorption. Somewhat larger differences are found for very thick clouds, and we hypothesise that the strong absorption in the oxygen A-band causes the POLDER instrument to retrieve lower pressures for those scenes.

1. Introduction

Clouds have a large influence on the transfer of radiation in the atmosphere. This makes clouds important in climate studies and for trace gas retrievals in passive remote sensing. For climate studies several properties are needed: particle phase, particle radius, cloud liquid- or ice-water content, cloud optical thickness, and cloud (top) pressure or cloud (top) temperature. These are usually observed using a combination of wavelength bands in the visible and thermal infra-red part of the spectrum. For the cloud correction of trace gas retrievals from UV/VIS reflectance spectra two much simpler cloud parameters are commonly used: an effective cloud fraction c_{eff} and a cloud pressure p_{c}. These parameters are found from a fit of the observed top-of-atmosphere reflectance, and the strength of a height-sensitive spectral feature. In the present article we compare cloud pressure data from two satellite instruments flying in the "A" train, using one month of data with global coverage.

This comparison includes three cloud products: cloud pressure derived from the O_2 A-band absorption at 760 nm, cloud pressure derived from O_2–O_2 absorption at 477 nm and cloud pressure derived from the filling in of Fraunhofer lines by rotational Raman scattering at 350 nm. The first is observed by the POLDER (Polarization and Directionality of the Earth's Reflectances) instrument on PARASOL (Polarization and Anisotropy of Reflectances for Atmospheric Sciences coupled with Observations from a Lidar), the latter two are observed from OMI (Ozone Monitoring Instrument) on Aura. The POLDER instrument is specifically designed to study cloud and aerosol properties from space, while

OMI is designed to measure high resolution reflectance spectra to perform atmospheric composition measurements.

The structure of this paper is as follows. The next section briefly described the two instruments, followed by a section on the cloud retrieval algorithms. Next is a short section on matching measurements from OMI to measurements from PARASOL, followed by a description of the actual comparison results. We end with a discussion of the similarities and differences we observe, and a brief discussion of future improvements.

2. Description of the instruments

Both Aura and PARASOL are part of the so called "A" train, a series of satellites carrying Earth observation instruments. Near the front of the train is the PARASOL satellite with its POLDER instrument, which will be described in brief detail in section 2.1. The last satellite in the A train is Aura, which carries four instruments, including OMI. This instrument is briefly described in section 2.2. Both instruments sample the same part of the atmosphere within approximately 15 minutes. PARASOL has a local equator crossing time of about 13:30, Aura crosses the equator at about 13:45.

2.1. Description of PARASOL/POLDER instrument

PARASOL is flying in formation with Aqua and Aura (NASA), CALIPSO (NASA/CNES) and CloudSat (NASA/CSA) as part of the A train. The PARASOL scientific objectives are to characterize the radiative and microphysical properties of clouds and aerosols using as best as possible the data complementarities from the different sensors on board the A train. PARASOL is carrying a wide-field imaging radiometer/polarimeter called POLDER. POLDER is designed to measure the directionality and polarization of light reflected by the Earth-atmosphere system. The POLDER instrument is extensively described by *Deschamps et al.* [1994]. It is a digital camera with a two-dimensional (274×242 pixels) charged coupled device (CCD) detector array, wide field of view telecentric optics and a rotating wheel carrying spectral and polarized filters (see Fig. 1). Similar POLDER instruments have already flown aboard the Japanese ADEOS-1 (1996–1997) and ADEOS-2 (2003) platforms. Contrary to those first versions of POLDER, for the PARASOL version the telecentric optics array has been turned 90 degrees to favor multidirectional viewing over daily global coverage. When the satellite passes over a target, up to 16 observations are realized (up to 14 with the previous configuration). The swath is now 1600 km (across track) corresponding to a maximum field of view of 114°. A 490 nm polarized channel was also put in place of the 443 nm one. Moreover a 1020 nm waveband has been added to conduct observations for comparison with data acquired by the lidar on CALIPSO. The spectral bands and the central wavelengths of POLDER aboard PARASOL are reported in Table 1.

This instrument presents original features since it is not only multispectral but also multidirectional and multipolarization. Algorithms dedicated to "Earth Radiation Budget, Water Vapor, and Clouds" were developed, taking into account these capabilities [*Buriez et al.*, 1997]. More particularly, the multi-polarization capability allows determining the cloud thermodynamic phase and the cloud top pressure, the multi-directionality improves the derivation of the cloud optical thickness and the estimate of the reflected flux, whereas the multi-spectrality allows deriving the cloud middle pressure and the clear-sky water vapor content. Daily products and monthly syntheses are produced at 20 km resolution (after cloud detection performed at full resolution, 6 km, and for every direction). The data archive starts from March 4th, 2005, and PARASOL is still operational at present time.

2.2. Description of OMI on Aura

The Ozone Monitoring Instrument (OMI) is a contribution of the Netherlands' Agency for Aerospace Programs (NIVR) in collaboration with the Finnish Meteorological Institute (FMI) to NASA's EOS Aura mission. OMI will continue the TOMS satellite data record for total ozone and other atmospheric parameters related to ozone chemistry and climate. The OMI instrument employs hyperspectral imaging in a pushbroom mode to observe solar backscattered radiation in the visible and ultraviolet. The observed spectra cover the wavelength range 270 nm to 500 nm, with a spectral resolution of 0.42 – 0.63 nm. The swath is wide enough to allow for global coverage in one day (14 orbits), with a spatial resolution of $13 \times 24\,\mathrm{km}^2$ for nadir observations. The spectral range and resolution of OMI allows for the retrieval of column amounts of atmospheric trace gases, like O_3, NO_2, SO_2, BrO, HCHO, cloud detection is needed to correct those trace gas retrievals for the presence of clouds.

OMI uses two 2-dimensional charged coupled device (CCD) detector arrays, one for the UV wavelength range (270 – 350 nm) and the second one for visible wavelengths (350 – 500 nm). On either CCD, one dimension is used for the separate wavelengths, while the perpendicular dimension is used for the 60 across track positions (see Fig. 2). Unlike GOME, Sciamachy and GOME-2, OMI has no scanning mirror and its response is made independent of the polarization of the detected radiation with the use of a polarization scrambler. A detailed description of the OMI instrument and its science objectives can be found in *Levelt et al.* [2006a, b].

3. Short overview of the cloud height retrieval algorithms

Two of the retrieval algorithms use absorption of radiation by oxygen to determine the height of clouds in the atmosphere, while the third uses the amount of rotational Raman scattering observed from the filling in of the Fraunhofer lines in the solar spectrum to determine the cloud pressure. They all use reflected sunlight, rather than thermal infrared emissions from clouds, as is done in most meteorological satellite retrieval techniques for cloud top temperature and cloud top pressure. The oxygen absorption feature used in the first two algorithms is rather different, as is the spectral resolution of both instruments.

3.1. POLDER cloud pressure retrieval using the oxygen A-band at 760 nm

Two different methods were developed to retrieve cloud pressure from POLDER data. The first one (cloud Rayleigh pressure) is based on the analysis of polarized reflected light at 490 nm, and is not discussed further in the present article. The second one (cloud oxygen pressure) uses the ratio of the two POLDER radiances measured in the oxygen A-band near 763 nm [*Buriez et al.*, 1997]. Cloud oxygen pressure p_{O_2} is determined from differential absorption between the radiances measured in the channels centered at 763 nm (narrow band) and 765 nm (wide band) respectively (see Fig. 3). The R_{763} and R_{765} radiances are first corrected for gaseous absorption of ozone and water vapor, then the measured oxygen transmittance T_{O_2} is obtained from the ratio of R_{763} and R_{765}. All the gaseous transmissions are derived from simulations using a line-by-line model [*Scott*, 1974]. The spectroscopic database used for the absorption cross sections is HITRAN 2004 [*Rothman et al.*, 2005]. In the first step, the influence of the surface albedo is neglected. An apparent pressure p_{app} is inferred by assuming that the atmosphere behaves as a pure absorbing medium overlying a perfect cloud reflector located at pressure

p_{app}. In practice, p_{app} is calculated from a polynomial function of T_{O_2} and the geometric air-mass factor $M = 1/\cos\theta + 1/\cos\theta_0$. The coefficients of the polynomials are fitted from line-by-line calculations.

Because of enhanced oxygen absorption due to the effects of surface reflection and multiple scattering inside the cloud, the apparent pressure p_{app} is almost always higher than the cloud top pressure. For example, even for optically thick clouds, large differences (typically 200 hPa) were observed between POLDER-1 apparent pressures and cloud top pressures derived from the brightness temperatures measured in the 11 µm channel of METEOSAT [*Vanbauce et al.*, 1998]. Comparable differences were observed between the apparent pressure and the Rayleigh pressure derived from POLDER polarization measurements [*Parol et al.*, 1999]. The apparent pressure can even be higher than the cloud base pressure when a great amount of photons reaches the surface before being reflected back to space, that is in the case of a thin cloud layer above a bright surface. Cloud oxygen pressure p_{O_2} is determined from the apparent pressure by removing the surface contribution. This correction is only realized for pixels over land surface, because the ocean reflectance is low at 765 nm and therefore the surface influence is negligible. Over sea-surface only viewing directions outside the sun-glint are retained. The scheme of the cloud oxygen pressure algorithm is given in Fig. 4. The starting point is that the oxygen A-band corresponds to strong absorption lines for which the oxygen transmission T_{O_2} can be treated by means of a random band model [*Goody*, 1964]:

$$T_{O_2} = \exp(-C\sqrt{M}p_{\text{app}}) \tag{1}$$

where M is the geometric air mass factor and C a constant depending on spectroscopic data. Considering that this transmission can be decomposed in a term corresponding to the light directly reflected by the cloud and a term corresponding to the light reflected after reaching the surface, the surface-corrected oxygen pressure can be written after some approximations (see *Vanbauce et al.* [2003] for details) in:

$$p_{O_2} = \frac{p_{app} + (r-1)p_{surface}}{r} \tag{2}$$

where r is the fraction of photons directly reflected by the cloud and $p_{surface}$ is the surface pressure. The fraction of photons reflected by the cloud, r, is calculated using $r = R^0_{765}/R_{765}$ where R_{765} is the reflectance measured by POLDER at 765 nm after correction for gaseous absorption and R^0_{765} is the reflectance that would be measured if in addition the surface was black. $p_{surface}$ is obtained from the ECMWF (European Center for Medium range Weather Forecasts) analysis. In the operational algorithm, p_{O_2} is calculated only for cloudy pixels with optical thickness larger than 3.5.

From comparisons of POLDER-1 cloud oxygen pressure and ARM/MMCR [*Clothiaux et al.*, 2000] cloud boundaries pressures, p_{O_2} appears to indicate the cloud middle pressure rather than the cloud top pressure [*Vanbauce et al.*, 2003].

3.2. OMI cloud pressure retrieval using the collision induced absorption at 477 nm

Only a brief overview of the OMI O_2–O_2 cloud model and cloud retrieval algorithm will be given here, since they are described in considerable detail in *Sneep et al.* [2007b] and *Acarreta et al.* [2004]. All atmospheric oxygen absorption bands (A, B, and γ bands, the oxygen transition $a\,^1\Delta_g(v = i) \leftarrow X\,^3\Sigma^-_g(v = 0)$ for $i = 0, 1, 2$, respectively) fall outside the wavelength range of OMI. This means that the FRESCO method for cloud height detection [*Koelemeijer et al.*, 2001], which is used for GOME and Sciamachy is not readily available for OMI. However, oxygen has several collision induced absorption (CIA) features within the OMI wavelength range, and they may be used instead. In these CIA features two oxygen molecules jointly absorb a single photon, and each fly away from the collision in an (electronically) excited state. The strongest of these CIA features within the OMI wavelength range is found at 477 nm, see for instance *Greenblatt et al.* [1990]. Because the absorption cross section of O_2–O_2 scales with the squared number density of oxygen, rather than directly with the oxygen number density as is the case for the oxygen A-band, some care is needed to correctly retrieve a cloud pressure from observations at 477 nm, and some different biases may be expected, compared to FRESCO or the POLDER oxygen cloud pressure.

A DOAS (Differential Optical Absorption Spectroscopy [*Platt*, 1994]) fit of the OMI reflectance spectrum between 460 and 490 nm is used to determine the slant column amount of O_2–O_2. This value, combined with the viewing- and solar geometry and surface conditions, is used to find the cloud pressure with the aid of a lookup table. The lookup table was produced with the DAK (Doubling Adding KNMI [*de Haan et al.*, 1987; *Stammes*, 2001]) radiative transfer model, using a Lambertian surface with albedo 0.8 as the cloud model. Simulations have shown that the pressure of the cloud retrieved by this method is at about the mid-level of the cloud [*Sneep et al.*, 2007b], even for optically thick clouds.

3.3. OMI cloud pressure retrieval using the filling in of Fraunhofer lines by rotational Raman scattering at 350 nm

Rotational-Raman scattering (RRS) causes filling-in and depletion of solar Fraunhofer lines throughout the ultraviolet in the observed backscattered Earth radiance (normalized by the solar irradiance) [e.g. *Joiner et al.*, 1995]. This property was first used to retrieve an effective cloud pressure by *Joiner and Bhartia* [1995]. Spectral fitting methods that exploit the high-frequency spectral structure of RRS have been applied to hyperspectral instruments such as GOME and OMI [*Joiner et al.*, 2004; *Vasilkov et al.*, 2004; *Joiner and Vassilkov*, 2006]. The latter reference contains a description of a soft-calibration procedure that is used to remove scan position-dependent biases (i.e. striping) from the retrieved cloud pressures.

The OMI RRS algorithm is currently implemented with the same cloud model as the OMI O_2–O_2 cloud retrieval algorithm, as described in section 3.4. There are two sets of products based on separate sets of assumptions applied to this model: The first set of products is included for historical reasons using a cloud albedo of 0.4 that produces an effective cloud fraction close to the MODIS geometrical cloud fraction. A second set is produced assuming a cloud albedo of 0.8 that gives cloud pressures closer to the physical cloud top at the lower cloud fractions. The latter set of products (called 'CloudPressureforO3' and 'CloudFractionforO3' in the OMCLDRR product files) is the one that will be used throughout this paper.

These products are generated assuming a fixed surface albedo of 0.15 that was chosen to be consistent with the OMI total ozone retrieval based on the Total Ozone Mapping Spectrometer (TOMS) version 8 algorithm. This value is known to be higher than the actual surface albedo under most conditions but was designed to account for aerosol and small amounts of low-level cloud in the OMI TOMS-V8. In an off-line study, we have applied the assumption of a 0.05 surface albedo to the OMCLDRR algorithm. We found that this assumption brings the cloud pressures into closer agreement with the OMI O_2–O_2 cloud algorithm especially at the lower cloud fractions.

3.4. Differences in the cloud models used by POLDER and OMI

Both OMI cloud products use basically the same cloud model, which is the same as the cloud model used in FRESCO [*Koelemeijer et al.*, 2001]. The cloud is represented by a Lambertian surface with albedo 0.8, no light is transmitted through the cloud. The scene is partially covered by the model cloud with an effective cloud fraction c_{eff}, so that the top-of-atmosphere reflectance agrees with the observed reflectance. The albedo of the model cloud is so high that most scenes have an effective cloud fraction less than one; the missing transmission of this model cloud is compensated by the large cloud-free part of the pixel. Comparisons with simulations of scattering clouds have shown that the albedo of 0.8 is a suitable value for this model cloud [*Koelemeijer and Stammes*, 1999; *Wang et al.*, 2006; *Vasilkov et al.*, 2007]. The cloud pressure is adjusted so that the retrieved cloud shows the same amount of signal (either O_2–O_2 slant column, or amount of Ring effect) as the observation.

The POLDER cloud model is different from the OMI cloud model, namely a scattering and transmitting cloud. Here the retrieval is limited to cloudy subpixels (6×6 km), where there is complete cloud cover with an optical thickness of 3.5 or larger. Over sea, where the surface is very dark at 760 nm, the cloud optical thickness is used as a threshold value in determining the cloud pressure. Over land, where the surface can be very bright at 760 nm, especially over vegetation, the cloud optical thickness is used both for selection and correction of p_{app}. The cloud pressures measured from different viewing angles are averaged, and then the results for the cloudy sub-pixels are combined with a cloud cover weighted mean into the final cloud pressure at $18 \times 18\,\mathrm{km}^2$ pixels.

4. Matching individual scenes in OMI and PARASOL

The pixels on which POLDER reports the cloud pressure are $18 \times 18\,\mathrm{km}^2$, comparable to the OMI nadir pixel size of $13 \times 24\,\mathrm{km}^2$. For this reason a one-to-one mapping between the two datasets was chosen, with a single PARASOL scene compared to one OMI scene. The PARASOL data is stored on a non-rectangular grid, and functions exist to map a (latitude, longitude) coordinate pair onto this grid. For each OMI pixel the matching PARASOL pixel is looked up, and stored on the OMI grid for later comparison. For this article a special dataset was prepared where each orbit is stored in a separate file, rather than the standard single day in an orbit. This was done to avoid overlap of successive orbits at higher latitudes.

5. Comparison results

For this comparison a total of 383 orbits were used (OMI orbit numbers 9986 to 10 422, PARASOL repeat cycle 34, orbit 219 to cycle 36, orbit 189), covering most of June 2006. The two instruments sample the same part of the atmosphere within about 15 minutes. The measurements were filtered to exclude pixels over a bright surface by excluding snow or ice covered surfaces. For these scenes it is known that the contrast between cloud cover and the surface is too low to properly distinguish clouds from the background, leading to an incorrect effective cloud fraction [*Sneep et al.*, 2007b], and therefore an ill-determined cloud pressure. Furthermore, the data was filtered to exclude pixels with a POLDER cloud cover less than 95 %, and pixels where the rotational Raman effective cloud fraction is less than 0.2, because the rotational Raman algorithm switches to a different cloud model in those cases. The OMI rotational Raman scattering cloud product comes in two flavors; here the "cloud pressure for O_3" was used exclusively.

Histograms showing the global distribution of cloud pressures from the three retrieval methods are shown in Fig. 5 separately for scenes over land and sea. Over sea a bi-modal pressure distribution is found, while over land only a single mode is observed. Although the overall shape of the distribution of cloud pressures is very similar, some differences can be seen. To investigate where these differences occur, separate histograms are made for small ($0.2 \leq c_{\text{eff}} < 0.4$) and large ($c_{\text{eff}} > 0.8$) effective cloud fractions (from the OMI O_2–O_2 algorithm) , shown in Fig. 6. The distributions of the differences between the three cloud pressures are shown in Fig. 7. These observations will be discussed in section 6.

Scatter plots of all combinations of the three parameters are shown in Fig. 8, again separated for land and sea. The correlation coefficient ρ and the slope from a straight line fit including the errors in both data sets, following *Press et al.* [2003, section 15.3], are listed in each of the sub-figures.

Fig. 9 shows the correlation coefficients, the median difference, and the 66 % quantile width between all three data sets over land and over sea as a function of the effective cloud fraction. An increase in correlation with increasing c_{eff} is seen for land and sea. The median difference shows some interesting behaviour which will be dicussed in section 6. The results are summarized in table 2.

6. Discussion

The three cloud pressure products are in good to excellent agreement, with average differences between them that are well within the stated accuracy of those products.

From other comparisons and model studies [*Vanbauce et al.*, 1998; *Koelemeijer et al.*, 2001; *Vanbauce et al.*, 2003; *Sneep et al.*, 2007b; *Vasilkov et al.*, 2007] it was already clear that the cloud pressure derived from visible or near infrared reflectance spectra is well within the cloud, and probably close to the mid-pressure level. This is in stark contrast to thermal infrared observations, where the cloud top pressure is retrieved. An exception to this rule is the cloud Rayleigh pressure from POLDER, where the degree of polarization at 490 nm is used, and the underlying assumption is that a cloud will scramble all polarization signal, yielding the top of the cloud layer, sometimes even above the cloud top pressure found by a thermal infrared instrument like MODIS [*Parol et al.*, 2006].

Not only are the average differences small, the correlation between the data sets is high and the slope observed in the scatter plots is reasonably close to 1, giving confidence in all algorithms involved. With measurements that are in such good agreement, there are details that tend to stand out, and those details will be discussed below.

From the distributions shown in Fig. 5, in particular over sea, one could conclude that the OMI O_2–O_2 cloud pressure retrieval is less sensitive for low pressure clouds than the O_2 A-band retrieval from PARASOL. One might expect that this is caused by the pressure dependence of the absorption strength of the collision induced absorption ($\sigma_{O_2\text{–}O_2} \propto p^2$). On the other hand, the rotational Raman scattering product does not have a similar pressure dependence, and yet it shows a similar behavior at low pressures compared to the OMI O_2–O_2 cloud pressures. Model studies presented in *Sneep et al.* [2007b] indicated that the expected influence of the quadratic pressure dependence of the absorption cross section is limited to approximately 40 hPa, which can not explain the median difference of ~100 hPa found here for thick clouds. Because the differences are most clearly seen over sea, we limited the next few steps to that subset.

Inspection of Fig. 5 for pixels over sea shows that for clouds at low pressures the PARASOL O_2 A-band algorithm retrieves smaller pressures than the OMI O_2–O_2 and RRS algorithms. A similar effect can be seen in Fig. 6 for pixels with a large effective cloud fraction. In these cases we deal presumably with convective clouds with the cloud top located at low pressures. The OMI RRS and O_2–O_2 algorithms need to put the Lambertian cloud at relatively high pressures, corresponding to pressures deep inside the scattering cloud, to reproduce the measured signal [*Vasilkov et al.*, 2007]. In contrast, the O_2 A-band algorithm can put the perfect reflector at lower pressures, closer to the cloud top, to reproduce the measured signal. Due to the relatively strong absorption in the O_2 A-band photons in this band may not penetrate as deeply inside the scattering cloud, while photons in the weakly absorbing O_2–O_2 band and photons affected by Raman scattering penetrate deep inside the scattering cloud. Therefore, the O_2–O_2 and RRS algorithms retrieve higher pressures than the O_2 A-band algorithm for these clouds. For optically thin clouds, which are probably also geometrically thin, photons can penetrate the entire cloud for all of the three algorithms. Therefore, similar distributions are found for the O_2 A-band and the O_2–O_2 band for small effective cloud fractions in Fig. 6. The deviating behaviour of RRS for thin clouds is believed to be caused by the assumed value of the surface albedo. In *Sneep et al.* [2007a] it is shown that the cloud pressures retrieved by the RRS method are much closer to the O_2–O_2 cloud pressures when an improved surface albedo is used for the RRS method.

From a qualitative comparison with CloudSat radar profiles, we hypothesise that the more frequent occurrence of clouds between 700 and 750 hPa in RRS, seen most clearly in the thick cloud distribution shown in Fig. 6, is caused by a combination of effects: 1) the surface albedo assumption in RRS, which causes it to be too low, 2) effects of the cloud model used, which could well be different for both OMI cloud products since there is more Rayleigh scattering at the wavelengths used for RRS, and differences in the way multi-layer cloud decks are handled. The presence of sun glint has opposing effects on both OMI products, causing a shoft towards low pressures for RRS and a shift towards the surface for O_2–O_2. The effect of sun glint on the present analysis was investigated, and while the correlation between the two OMI cloud pressures improved slightly at low cloud fractions, no significant changes in the statistical results were obeserved. More research, including radiative transfer calculations in geometrically thick clouds and multiple cloud decks, are needed to understand the differences between the algorithms.

7. Conclusions and outlook

The cloud pressures retrieved from OMI and POLDER measurements using oxygen absorption or the amount of rotational Raman scattering to determine the cloud height find remarkably similar cloud heights. In general the cloud pressure measured by these methods is much higher than the cloud pressure derived from thermal infrared measurements. Model studies and comparisons with ground based radar profiles [*Vanbauce et al.*, 1998; *Koelemeijer et al.*, 2001; *Vanbauce et al.*, 2003; *Sneep et al.*, 2007b; *Vasilkov et al.*, 2007] suggest that the cloud pressures retrieved here indicate the mid-level of the cloud layer.

Despite the good agreement, there are some differences visible between the three algorithms, due to different sensitivities and different assumptions used at various stages in the retrieval. The OMI O_2–O_2 algorithm uses a monthly surface albedo climatology derived from GOME measurements at $1° \times 1.25°$, while the rotational Raman scattering algorithm uses a fixed value for the surface albedo of 0.15 which comes from the TOMS heritage. In a future version both will switch to a surface albedo climatology derived from OMI measurements at $0.25° \times 0.25°$. This will affect the cloud fraction most directly, but a change in effective cloud fraction will change the cloud pressure because the same strength of the spectral feature needs to be explained.

The strength of the oxygen A-band leads to a different sensitivity to the cloud optical- and geometrical thickness when compared to the much weaker oxygen collision induced absorption at 477 nm or rotational Raman scattering near 350 nm. This difference affects the retrieved cloud pressure for scenes with a high effective cloud fraction, where POLDER retrieves a pressure closer to the cloud top than the other two algorithms.

Acknowledgments. The OMI and PARASOL science teams are gratefully acknowledged. The work at KNMI was funded by the Space Research Organisation of the Netherlands (SRON) under grant number EO-072. The work at Laboratoire d'Optique Atmosphérique (LOA) was supported by the Centre National d'Etudes Spatciales (CNES) and Région Nord-Pas de Calais. Joiner and Vasilkov acknowledge support from NASA under funding for the OMI science team. Discussions with Ping Wang are acknowledged.

References

Acarreta, J. R., J. F. de Haan, and P. Stammes, Cloud pressure retrieval using the O_2–O_2 absorption band at 477 nm, *J. Geophys. Res.*, *109*, D05,204, 2004.

Buriez, J., C. Vanbauce, F. Parol, P. Goloub, M. Herman, B. Bonnel, Y. Fouquart, P. Couvert, and G. Sèze, Cloud detection and derivation of cloud properties from POLDER, *Int. J. Remote Sens.*, *18*, 2785–2813, 1997.

Clothiaux, E. E., T. P. Ackerman, G. G. Mace, K. P. Moran, R. T. Marchand, M. A. Miller, and B. E. Martner, Objective determination of cloud heights and radar reflectivities using a combination of active remote sensors at the ARM CART sites, *J. Appl. Meteor.*, *39*, 645–665, 2000.

de Haan, J. F., P. B. Bosma, and J. W. Hovenier, The adding method for multiple scattering calculations of polarized light, *Atron. Astrophys.*, *183*, 371–393, 1987.

Deschamps, P., F. Breon, M. Leroy, A. Podaire, A. Bricaud, J.-C. Buriez, and G. Sèze, The POLDER mission: Instrument characteristics ans scientific objectives, *IEEE Trans. Geosci. Rem. Sens.*, *32*, 598–615, 1994.

Goody, R. M., *Atmospheric Radiation I. Theoretical Basis*, Clarendon Press, Oxford, 1964.

Greenblatt, G. D., J. J. Orlando, J. B.Burkholder, and A. R. Ravishankara, Absorption measurements of Oxygen between 330 and 1140 nm, *J. Geophys. Res.*, *95*, 18,577–18,582, 1990.

Joiner, J., and P. K. Bhartia, The determination of cloud pressures from rotational Raman scattering in satellite backscatter ultraviolet measurements, *J. Geophys. Res.*, *100*, 23,019–23,026, 1995.

Joiner, J., and A. P. Vassilkov, First results from the OMI rotational Raman scattering cloud pressure algorithm, *IEEE Trans. Geosci. Rem. Sens.*, *44*, 1272–1282, 2006.

Joiner, J., P. K. Bhartia, R. P. Cebula, E. Hilsenrath, R. D. McPeters, and H. Park, Rotational-Raman scattering (Ring effect) in satellite backscatter ultraviolet measurements, *Appl. Opt.*, *34*, 4513, 1995.

Joiner, J., A. P. Vasilkov, D. E. Flittner, J. F. Gleason, and P. K. Bhartia, Retrieval of cloud pressure and oceanic chlorophyll content using Raman scattering in GOME ultraviolet spectra, *J. Geophys. Res.*, *109*, D01,109, 2004.

Koelemeijer, R. B. A., and P. Stammes, Effects of clouds on ozone column retrieval from GOME UV measurements, *J. Geophys. Res.*, *104*, 8281–8294, 1999.

Koelemeijer, R. B. A., P. Stammes, J. W. Hovenier, and J. F. de Haan, A fast method for retrieval of cloud parameters using oxygen A-band measurements from GOME, *J. Geophys. Res.*, *106*, 3475–3490, 2001.

Levelt, P. F., E. Hilsenrath, G. W. Lepppelmeier, G. H. J. van den Oord, P. K. Bhartia, J. Taminnen, J. F. de Haan, and J. P. Veefkind, Science objectives of the Ozone Monitoring Instrument, *IEEE Trans. Geosci. Rem. Sens.*, *44*, 1199–1208, 2006a.

Levelt, P. F., G. H. J. van den Oord, M. R. Dobber, A. Malkki, H. Visser, J. de Vries, P. Stammes, J. Lundell, and H. Saari, The Ozone Monitoring Instrument, *IEEE Trans. Geosci. Rem. Sens.*, *44*, 1093–1101, 2006b.

Parol, F., J.-C. Buriez, C. Vanbauce, P. Couvert, G. Sèze, P. Goloub, , and S. Cheinet, First results of the POLDER "Earth Radiation Budget and Clouds" operational algorithm, *IEEE Trans. Geosci. Rem. Sens.*, *37*, 1597–1612, 1999.

Parol, F., J. Buriez, C. Vanbauce, J. Riedi, C. Cornet, F. Thieuleux, C. Oudard, G. Sèze, and Z. Poussi, Cloud property retrievals from POLDER onboard the PARASOL platform, European Geophysical Union General Assembly, Vienna, Austria, 2006.

Platt, U., Differential optical absorption spectroscopy (DOAS), in *Air monitoring by spectroscopic techniques*, edited by M. W. Sigrist, vol. 127 of *Chemical Analysis Series*, chap. 2, pp. 27–84, John Wiley & Sons, 1994.

Press, W. H., S. A. Teukolsky, W. T. Vetterling, and B. P. Flannery, *Numerical recipes in Fortran 77: The Art of Scientific Computing*, 2 ed., Press syndicate of the University of Cambridge, 2003.

Rothman, L. S., et al., The HITRAN 2004 molecular spectroscopic database, *J. Quant. Spectrosc. Radiat. Transfer*, *96*, 139–204, 2005.

Scott, N. A., A direct method of computation of the transmission function of an inhomogeneous gaseous medium. I: description of the method, *J. Quant. Spectrosc. Radiat. Transfer*, *14*, 691–704, 1974.

Sneep, M., J. Joiner, A. Vasilkov, and P. Stammes, Evaluation of the OMI cloud products, *J. Geophys. Res.*, 2007a, to be published in the same issue as this article.

Sneep, M., P. Stammes, J. P. Veefkind, J. F. de Haan, B. Veihelmann, and P. F. Levelt, Comparison of the OMI O_2–O_2 cloud product with MODIS/Aqua cloud products, *J. Geophys. Res.*, 2007b, to be published in the same issue as this article.

Stammes, P., Spectral radiance modeling in the UV-visible range, in *IRS200: Current problems in atmospheric radiation*, edited by W. L. Smith and Y. M. Timofeyev, pp. 385–388, A. Deepak, Hampton, Va., 2001.

Vanbauce, C., J. Buriez, F. Parol, B. Bonnel, G. Sèze, and P. Couvert, Apparent pressure derived from ADEOS-POLDER observations in the oxygen A-band over ocean, *Geophys. Res. Lett.*, *25*, 3159–3162, 1998.

Vanbauce, C., B. Cadet, and R. Marchand, Comparison of POLDER apparent and corrected oxygen pressure to ARM/MMCR cloud boundary pressures, *Geophys. Res. Lett.*, *30*, 1212, 2003.

Vasilkov, A. P., J. Joiner, K. Yang, and P. K. Bhartia, Improving total column ozone retrievals by using cloud pressures derived from Raman scattering in the UV, *Geophys. Res. Lett.*, *31*, L20,109, 2004.

Vasilkov, A. P., J. Joiner, R. Spurr, P. K. Bhartia, P. F. Levelt, and G. Stephens, Evaluation of the OMI cloud pressures derived from rotational Raman scattering by comparisons with other data and radiative transfer simulations, *J. Geophys. Res.*, 2007.

Wang, P., P. Stammes, and K. F. Boersma, Impact of the effective cloud fraction assumption on tropospheric NO_2 retrievals, in *Proceedings of the first conference on atmospheric science*, SP-628, ESA, 2006.

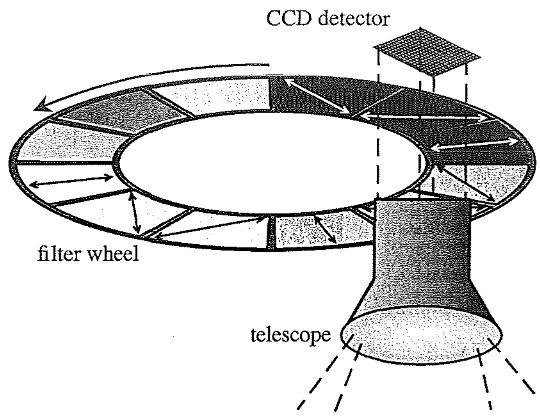

Figure 1. The measurement principle of POLDER on PARASOL.

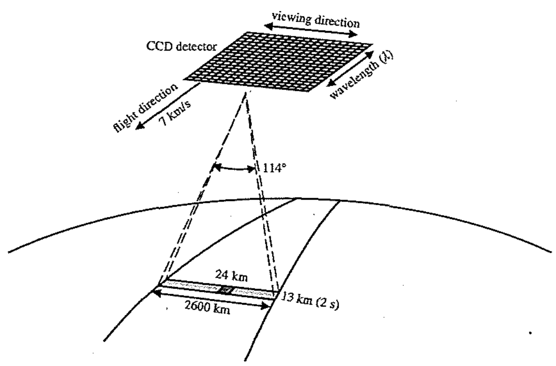

Figure 2. The measurement principle of OMI.

Table 1. The spectral bands in POLDER on PARASOL. Channels labeled with (P) measure polarization.

Channel	Bandwidth	Rationale
443 nm	20 nm	Ocean color applications
490 nm (P)	20 nm	Cloud properties, Aerosol retrieval
565 nm	20 nm	Calipso lidar at 532 nm
670 nm (P)	20 nm	Aerosol retrieval, Cloud properties
763 nm	10 nm	Cloud oxygen pressure by differential
765 nm	40 nm	absorption in oxygen A-band
865 nm (P)	40 nm	Aerosol retrieval, Cloud properties
910 nm	20 nm	Water vapor retrieval
1020 nm	20 nm	Calipso lidar at 1064 nm, Aerosol retrieval

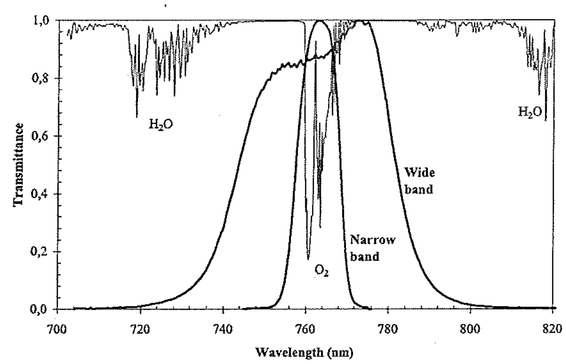

Figure 3. POLDER/PARASOL filter transmissions in the narrow and wide bands centered at 763 nm and 765 nm, respectively, together with atmospheric transmission in the oxygen A-band region.

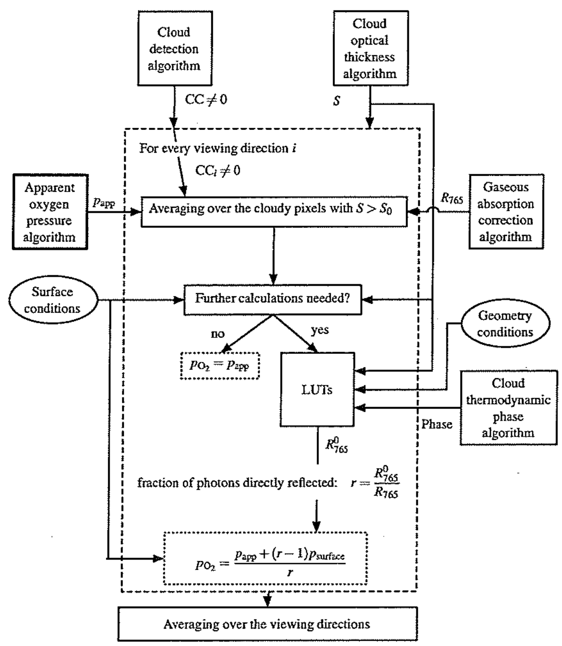

Figure 4. Scheme of the POLDER cloud oxygen pressure algorithm.

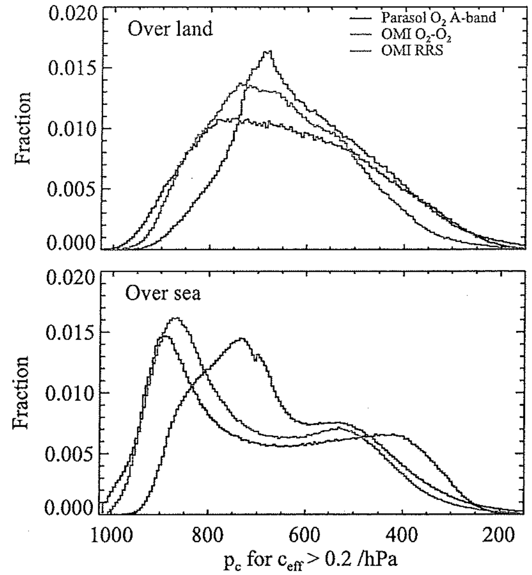

Figure 5. The distributions of cloud pressures from the OMI O_2–O_2, the OMI rotational Raman scattering, and the POLDER on PARASOL O_2 A-band products, for scenes over land (top) and sea (bottom).

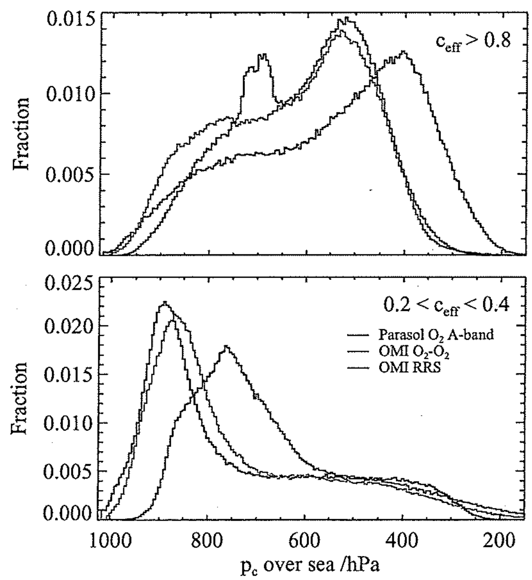

Figure 6. The distribution of cloud pressures from the OMI O_2–O_2, the OMI rotational Raman scattering, and the POLDER on PARASOL O_2 A-band products, over sea for scenes with a large effective cloud fraction (top) and scenes with a small effective cloud fraction (bottom).

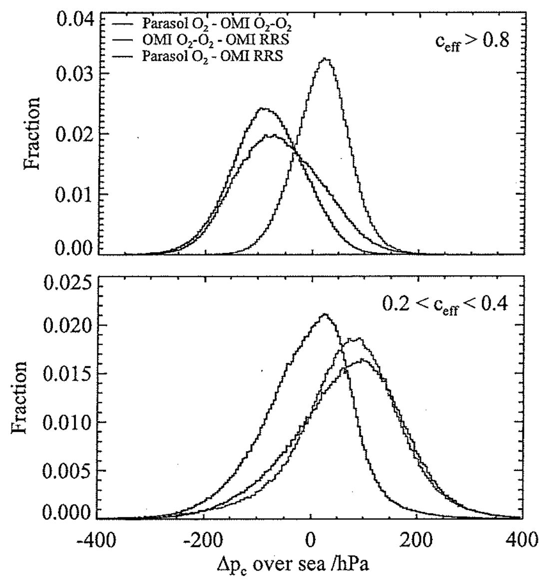

Figure 7. The distribution of differences in the cloud pressure between the O_2–O_2 cloud pressure, the rotational Raman scattering, both from OMI on EOS Aura and the oxygen cloud pressure from POLDER on PARASOL for colocated scenes over sea, for scenes with a large effective cloud fraction (top) and scenes with a small effective cloud fraction (bottom).

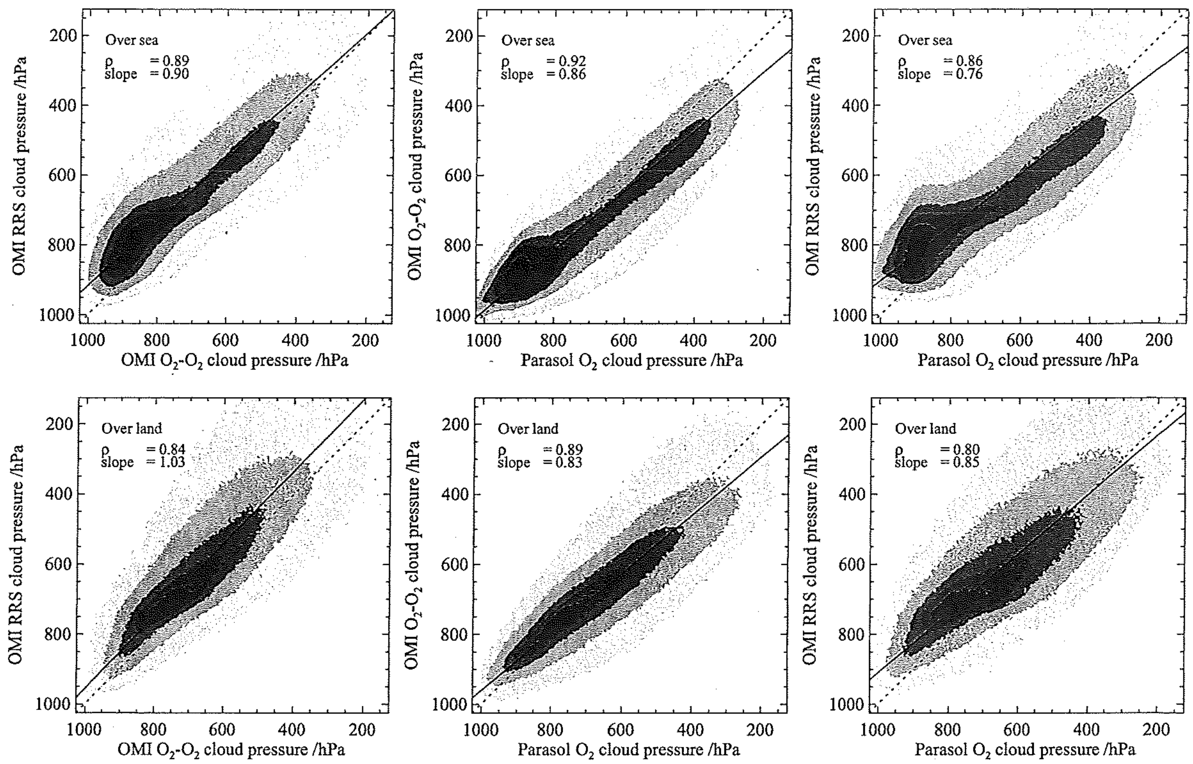

Figure 8. Probability distribution of the cloud pressure determined from OMI and PARASOL. The contours represent the densest area in the scatter plot, with the contours containing 10 %, 30 %, 60 %, 90 %, and 99 % of all points, going to progressively lighter colors, for each of the three combinations of two algorithms. The data is shown separately for land and sea surfaces. The dotted line in each of the plots are the $x = y$ relation, the drawn line is the result of an orthogonal regression analysis, the slope of which is printed in each plot.

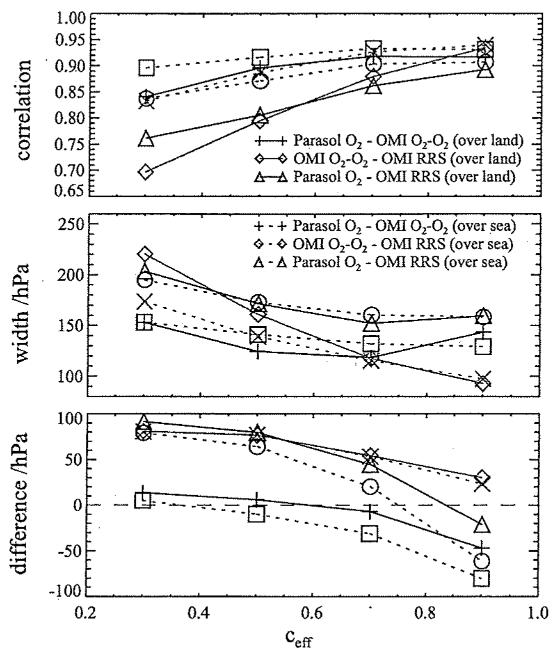

Figure 9. Correlation, 66 % central quantile width and median difference between all three combinations of cloud pressure products, over both land (drawn lines) and sea (dashed lines), plotted as a function of the effective cloud fraction. The measurements were grouped by c_{eff}, from 0.2 to 0.4, from 0.4 to 0.6, from 0.6 to 0.8, and 0.8 and larger.

Table 2. Some statistical parameters describing the differences of the co-located cloud pressure retrievals. The difference is the product listed at the top minus the product listed at the left, the slope is for the product listed at the top projected on the horizontal axis. This is for pixels over land and sea combined, filtered to include only pixels with $c_{\text{eff}} > 0.5$.

	POLDER O_2 A	OMI O_2–O_2	OMI RRS
POLDER O_2 A		$\overline{\Delta p_c} = 45\,\text{hPa}$ $\sigma(\Delta p_c) = 74\,\text{hPa}$ $\rho = 0.93$ slope = 1.19	$\overline{\Delta p_c} = 2\,\text{hPa}$ $\sigma(\Delta p_c) = 93\,\text{hPa}$ $\rho = 0.88$ slope = 1.32
OMI O_2–O_2	$\overline{\Delta p_c} = -45\,\text{hPa}$ $\sigma(\Delta p_c) = 74\,\text{hPa}$ $\rho = 0.93$ slope = 0.84		$\overline{\Delta p_c} = -44\,\text{hPa}$ $\sigma(\Delta p_c) = 65\,\text{hPa}$ $\rho = 0.92$ slope = 1.09
OMI RRS	$\overline{\Delta p_c} = -2\,\text{hPa}$ $\sigma(\Delta p_c) = 93\,\text{hPa}$ $\rho = 0.88$ slope = 0.76	$\overline{\Delta p_c} = 44\,\text{hPa}$ $\sigma(\Delta p_c) = 65\,\text{hPa}$ $\rho = 0.92$ slope = 0.92	
$\overline{p_c}$	642 hPa	687 hPa	644 hPa